Analysis and control of DC drift in LiNbO3-based Mach-Zehnder modulators

Jean-Paul Salvestrini, Laurent Guilbert, Marc Fontana, Mustapha Abarkan, Stéphane Gille

Analysis and Control of the DC Drift in LiNbO -Based Mach–Zehnder Modulators

Jean Paul Salvestrini, Laurent Guilbert, Marc Fontana, Mustapha Abarkan, and Stéphane Gille

***Abstract*—The drift issue induces slow drifting of the optimum operating point for high efficiency or large nonlinearities in analog optical links, and requires complex control of the offset bias voltage for achieving high extinction ratio in digital optical links. We discuss and analyze the different sources of the drift in commercially $LiNbO_3$ Mach–Zehnder modulators. The different extrinsic and intrinsic origins are compared in terms of phase shift and the different corresponding orders of magnitude are given, pointing out the predominant role of the intrinsic (dc) drift. We show the large role played by the electrical inhomogeneities at the surface of the $LiNbO_3$ substrate by highlighting the link between the time dependence of the dc drift and the electrical conductivity measured at the surface and in the volume of the $LiNbO_3$ substrate. This allows to propose a solution to the drift issue which consists in the engineering of the electrical conductivity of the lithium niobate substrate.**

***Index Terms*—Drift, integrated optics, lithium niobate (LN), optical intensity modulator.**

I. Introduction

Intensity, phase, frequency, and polarization are various characteristics of a lightwave that can be modulated to carry information. Intensity modulation is the most used in optical fiber communication systems. Both analog and digital modulation systems requires high optical power handling capability, small optical loss, polarization insensitivity, and stable performance over ambient temperature variation and time. For high modulation frequency, the use of directly modulated semiconductor lasers is limited by relative intensity noise, signal distortions, and large frequency chirp. External modulation can minimize these effects. Several types of external optical intensity modulators have been developed over the past several decades for optical fiber communication applications.

Among them lithium niobate (LN) Mach–Zehnder (MZ) modulator is still considered as the device with the best performance [1]. The most remarkable advantages are the low optical loss, the high optical power handling capability, the broad optical bandwidth, and the zero or tunable chirp. The largest drawback for LN MZ modulator concerns the bias-drift issue which causes slow drift of the optimum bias point for high slope efficiency in analog links, and makes difficult the offset bias voltage adjustment for achieving high extinction ratio in digital links. This issue has received large attention these last decades. Bias drift rates differing by several orders of magnitude have been observed in both short and long duration experiments. A large number of explanations and solutions have been proposed. Nevertheless, there is still a lot of work to identify and understand the fundamental details of the mechanisms influencing bias stability.

The drift in an LN device may occur for several reasons. Extrinsic sources of drift are due to changes of environmental conditions including, for example, temperature, humidity, or stress. Under some conditions, such as with optical sources of shorter wavelength and high power, photoinduced processes may also contribute to bias point drift. Several techniques for reducing the effect of these extrinsic sources of bias drift are known. Furthermore, the intrinsic origin of the drift, related to the flow and redistribution of electrical charge in the device structure under the application of the voltage was not widely investigated. To our knowledge, only two alternative approaches have been proposed to attempt to solve this issue. The first one consists in finding empirically the desirable fabrication techniques [2] to obtain modulators with reduced drift. However, such improved devices still need further investigations from the viewpoint of the drift mechanism and production repeatability. On contrary, the second method is based on a careful analysis of the material layers constituting the device structure, via a general resistor–capacitor (RC) circuit model of the structure [3]. This model provides a means of assessing the magnitude of the changes required to reduce drift rates to a desired level, to gauge the effects of fabrication variations, and can suggest which elements are most critical.

Neither of these approaches is up to now satisfactory. While so far most LN devices display adequate stability for thousands of hours of continuous operation under bias, these systems require the optimal bias to remain within the output range of an automatic biasing circuit for durations up to ten thousand hours. To maintain the optimum voltage, it is common to employ some voltage control circuitry. The conventional approach is to use a weak low-frequency pilot-tone combined with the modulation signal. A *Y*-branch coupler has to be inserted after the modulator to bring a small portion of the output to a photodetector for checking the pilot-tone signal, so that the optimum voltage can be maintained for both analog and digital applications [4],

J. P. Salvestrini, L. Guilbert, and M. Fontana are with the Laboratoire Materiaux Optiques, Photonique et Systemes, Universite Paul Verlaine—Metz et Supelec, Metz 57070, France (e-mail: salvestr@metz.supelec.fr; guilbert@metz.supelec.fr; fontana@metz.supelec.fr).

M. Abarkan is with the Laboratoire Informatique, Mathematique, Automatique et Optoelectronique Faculte Polydisciplinaire de Taza, Taza B.P. 1323, Marocco (e-mail: mustapha_abarkan@yahoo.fr).

S. Gille was with the Laboratoire Materiaux Optiques, Photonique et Systemes, Universite Paul Verlaine—Metz et Supelec, Metz 57070, France. He is now with French Research and Safety Institute, Vandoeuvre 54501, France (e-mail: Stephane.Gille@lne.fr).

TABLE I
CLASSIFICATION OF THE DIFFERENT SOURCES OF THE DRIFT PHENOMENON IN LN MZ OPTICAL MODULATORS

SOURCE	PHYSICAL PARAMETER	PHYSICAL PROPERTIES	INDUCED EFFECT
EXTRINSIC	- Temperature	- Thermooptic and pyroelectric effects	Unstable phase shift
	- Optical power	- Photorefractive effect	
	- Mechanical stress	- Strain optic effect	
INTRINSIC	- Bias voltage	- Electrical relaxation	Unstable electric field

[5]. However, the use of this technique leads to the increase of both optical losses and complexity of the system.

In this paper, we will first discuss and analyze the different sources of the drift in commercially available LN MZ modulators (these devices are described in Appendix I-A). The different origins will be compared in terms of phase shift and the different corresponding orders of magnitude will be given, pointing out the predominant role of the intrinsic source of drift. Then, we will show the large influence of the electrical inhomogeneities at the surface of the LN substrate by highlighting the link between the time dependence of the dc drift in an LN MZ modulator and the electrical conductivity at the surface and in the volume of the LN substrate. Finally, we will describe briefly the solution that we propose, which consists in the engineering of the electrical conductivity of the LN substrate surface in order to suppress the long-term dc drift.

II. DIFFERENT SOURCES OF DRIFT IN LN MZ MODULATORS AND THEIR RELATIVE MAGNITUDES

The available results obtained by different groups suggest that the drift phenomenon is a complex problem. In [6], the time dependence of the drift, recorded during several thousands of hours in the case of *z*-cut titanium-diffused waveguide, exhibits large drift amplitude with different rates and nonmonotonic evolution. According to results obtained by Maack [7], the drift is similarly observed for devices based on *x*-cut LN substrate, for both titanium-diffused or proton-exchanged waveguides and with or without bias applied voltage. Nagata and Honda [8] have shown a strong dependence of the drift with the initial bias applied to the LN MZ modulators. The higher is the initial bias voltage, the higher is the drift. It is to be noticed that the drift amplitude is larger for biased modulators and that the time evolution of the drift measured in a set of modulators differs from one device to the other. As shown by Minford [9], the temperature plays an important role in the drift behavior in *z*-cut titanium-diffused waveguide devices, since the different drift rates decrease when the temperature of the modulator increases. These results are confirmed by the fact that the temperature dependence of the drift rate in *x*-cut or *z*-cut LN MZ modulators follows Arrhenius distribution [10], [11]. The silica buffer layer has also a large influence on the drift. The decrease of contaminants concentration such as H^+, Na^+, and K^+ ions in the silica layer was shown to reduce drastically the drift amplitude [10], [12]–[14].

The drift phenomenon originates from both extrinsic and intrinsic sources. The extrinsic origins of the drift are linked to the change of the effective refractive index of the optical mode of the waveguide via the possible variations of the temperature of the device (thermo-optic and pyroelectric effects), of the optical power in the waveguide (photorefractive effect) and the strain relaxation at the silica buffer-substrate interface (strain-optic effect). A classification of the different sources of the drift in LN MZ modulators is summarized in Table I and the different extrinsic origins are summarized and analyzed in Appendix II from the studies reported in the literature.

To evaluate the relative importance of each physical effect playing a role in the drift, we calculate the corresponding induced phase shift $\Delta\phi$ and we derive the value of the drift-magnitude $S(t)$ (see details in Appendix I-B) as

$$S(t) = \frac{2\Delta\phi}{\pi} \tag{1}$$

for each drift source. For this, we first have to consider the symmetry of both the waveguides constituting the MZ interferometer and the excitation (temperature, optical power, mechanical strain, etc.) change itself. The unbalanced interferometer can be characterized by a length difference δ between the two arms. Table II gives the expressions of the calculated phase shifts for the different cases.

We can note that the various extrinsic physical effects induce a drift of the operating point of the MZ modulator in all cases except if the device is symmetrical and if the excitation is the same in both arms of the MZ interferometer. Using (1), Table II and the values of the different physical constants of LN given in Appendix III, we have then calculated the drift magnitude S for unbalanced arms ($\delta = 1.3$ μm) and in the case of a symmetrical excitation ($\Delta T = 0.01$ K, $I_3 \propto |E_{3,A}|^2 = 10$ mW at $\lambda = 1.55$ μm, $\sigma = 10^{-5}$ N/m^2). The corresponding values of S are shown in Table III. We can see that both photoinduced and strain-optic drift exhibit a low value of the drift magnitude S. In contrary, a small temperature gradient between the two arms of the MZ modulator induces a large value of S indicating that the thermal drift is predominant in extrinsic sources of the drift. Nevertheless, these extrinsic drift amplitudes, when compared to drift amplitude reported in the literature and which can reach a value of S equal to more than 100%, are of weak importance especially if the MZ modulator is temperature controlled. Thus, for an optimal operating of the device, the issue of dc drift must be overcome. In that way, Section III and Section IV are devoted

TABLE II

CALCULATED INDUCED PHASE SHIFTS IN z-CUT LN MZ MODULATOR WAVEGUIDES LEADING TO A DRIFT OF THE OPERATING POINT OF THE DEVICE. L IS THE LENGTH OF THE ARMS OF THE INTERFEROMETER AND δ IS THE LENGTH DIFFERENCE BETWEEN THE TWO ARMS IN THE CASE OF AN UNBALANCED DEVICE. $r_{33}, p_{31}, (\delta n)/(\delta T)$, AND β_{33} ARE, RESPECTIVELY, THE ELECTRO-OPTIC, ELASTO-OPTIC, THERMO-OPTIC, AND PHOTO-VOLTAIC COEFFICIENTS OF LN. P_s, n_e, σ_d, AND $\sigma_{\rm ph}$ ARE, RESPECTIVELY, THE SPONTANEOUS POLARIZATION, REFRACTIVE INDEX, ELECTRICAL DARK, AND PHOTOCONDUCTIVITIES. THE EXCITATION SOURCES ARE THE TEMPERATURE VARIATION ΔT FOR THE THERMAL DRIFT, THE LIGHT INTENSITY $I \propto |E|^2$ FOR THE PHOTOINDUCED DRIFT AND THE MECHANICAL DEFORMATION s_1 FOR THE STRAIN-INDUCED DRIFT. A AND B CORRESPOND TO THE DIFFERENT ARMS OF THE MZ INTERFEROMETER. IN THE CASE OF BOTH SYMMETRICAL EXCITATION AND ARMS, THE INDUCED PHASE SHIFTS ARE NULL

	Symmetric excitation / Asymmetric arms	Asymmetric excitation / Symmetric arms	Asymmetric excitation / Asymmetric arms
Thermooptic effect	$\frac{2\pi\delta}{\lambda}\frac{\partial n}{\partial T}\Delta T$	$\frac{2\pi L}{\lambda}\frac{\partial n}{\partial T}(\Delta T_A\text{-}\Delta T_B)$	$\frac{2\pi L}{\lambda}\frac{\partial n}{\partial T}\ [L(\Delta T_A\text{-}\Delta T_B)+\delta\Delta T_A]$
Pyroelectric effect	$\text{-}\frac{\pi\delta}{\lambda}n_e^3 r_{33}\frac{\partial P_s}{\partial T}\frac{1}{\epsilon_0\epsilon_{33}}\Delta T$	$-\frac{\pi L}{\lambda}n_e^3 r_{33}\frac{\partial P_s}{\partial T}\ \frac{1}{\epsilon_0\epsilon_{33}}(\Delta T_A\text{-}\Delta T_B)$	$-\frac{\pi}{\lambda}n_e^3 r_{33}\frac{\partial P_s}{\partial T}\ \frac{1}{\epsilon_0\epsilon_{33}}[L(\Delta T_A\text{-}\Delta T_B)+\delta\Delta T_A]$
Photorefractive effect	$\text{-}\frac{\pi\delta}{\lambda}n_e^3 r_{33}\frac{1}{\sigma_d+\sigma_{ph}}\beta_{33}\lvert E_3\rvert^2$	$\text{-}\frac{\pi L}{\lambda}n_e^3 r_{33}\frac{1}{\sigma_d+\sigma_{ph}}\beta_{33}(\lvert E_{3,A}\rvert^2\text{-}\lvert E_{3,B}\rvert^2)$	$\text{-}\frac{\pi}{\lambda}n_e^3 r_{33}\frac{1}{\sigma_d+\sigma_{ph}}\beta_{33}[L(\lvert E_{3,A}\rvert^2\text{-}\lvert E_{3,B}\rvert^2)+\delta\lvert E_{3,A}\rvert^2]$
Strainoptic effect	$\text{-}\frac{\pi\delta}{\lambda}n_e^3 p_{31}s_1$	$\text{-}\frac{\pi L}{\lambda}n_e^3 p_{31}(s_{1A}\text{-}s_{1B})$	$\text{-}\frac{\pi L}{\lambda}n_e^3 p_{31}(s_{1A}\text{-}s_{1B})\text{-}\frac{\pi\delta}{\lambda}n_e^3 p_{31}s_{1A}$

TABLE III

ESTIMATION OF THE RELATIVE MAGNITUDE OF THE DRIFT MAGNITUDE S ORIGINATING FROM THE EXTRINSIC SOURCES IN AN LN MZ OPTICAL MODULATORS WITH ASYMMETRIC ARMS AND IN THE CASE OF A SYMMETRIC EXCITATION

	THERMAL DRIFT	PHOTO-INDUCED DRIFT	STRAIN OPTIC DRIFT
DRIFT-MAGNITUDE S	6 %	10^{-5} %	4 10^{-2} %
VALUES OF THE PARAMETERS	ΔT = 0.01 K, δ = 1.3 μm	λ=1.55μm, E_3^2=10mW, δ=1.3 μm	δ=1.3 μm, σ=10^{-5}N/m^2

to a detailed analysis and description of the electrically induced drift as well as to a possible solution.

III. INTRINSIC OR ELECTRICALLY INDUCED DRIFT

The intrinsic source of the drift phenomenon originates from electrical charge relaxation due to both the inhomogeneous material structure (silica buffer layer, Ti:LN waveguide, LN substrate), the electrically anisotropic LN substrate and the inhomogeneous electrical properties (especially the electrical conductivity) at the surface of the substrate. The latter can appear during the waveguide fabrication process (titanium diffusion or proton exchange). These electrical inhomogeneities lead, when the bias voltage is applied, to a redistribution of the electrical charges yielding the appearance of a time-dependent depolarizing electric field.

A schematic view of a z-cut LN MZ modulator is represented in Fig. 1. When a voltage is applied between the $+$ and $-$ electrodes, the time evolution of the electric field in such a structure is described and can be derived by solving the following system of equations:

$$\begin{aligned} \text{div}\,([\epsilon]\vec{E}) &= \rho \\ \text{div}\,([\sigma]\vec{E}) &= -\frac{\partial\rho}{\partial t} \end{aligned} \qquad (2)$$

where $[\epsilon]$, and $[\sigma]$ are, respectively, the dielectric permittivity and electrical conductivity tensors, and ρ is the electrical charge density.

The system of (2) shows clearly that the fact that either of the dielectric permittivity and/or the electrical conductivity and/or the applied electric field are inhomogeneous leads to a time-dependent electrical charges distribution inside the structure of the device, and then to an electric field that evolves with time

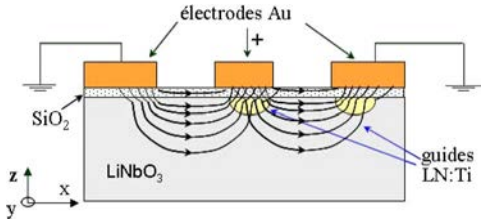

Fig. 1. Schematic cross-sectional view of a z-cut $LiNbO_3$ MZ modulator.

inducing a drift of the operating point of the LN MZ modulator. In addition to the electrical inhomogeneity of the structure, inhomogeneities of the different layers themselves have to be considered (silica buffer, anisotropic LN substrate, and top surface of the substrate in the waveguides region). To facilitate progress on the understanding and engineering of the bias stability of the component, several *RC* models have been proposed [3], [12], [13]. Circuits composed of resistances and capacitances were chosen to model how the charges distribution, and thus the electric field, evolves with time. Using very simple circuits, Yamada and Minakata [12] discussed charge storage in oxide buffer layers, whereas Becker [13] is focused only on the role of the built-in electrical anisotropy of the $LiNbO_3$ substrate. In [3], using a quite complicated circuit, buffer layer, substrate, and waveguide region of the substrate were taken into account.

A. Theoretical Approach

Our present approach is similar to [12] and [13]. In contrast to [3], where as many *RC* circuits as necessary to describe correctly the time dependence of the experimentally recorded drift magnitude $S(t)$ are introduced, our model is based on only three *RC* circuits corresponding to both buffer layer and the anisotropy

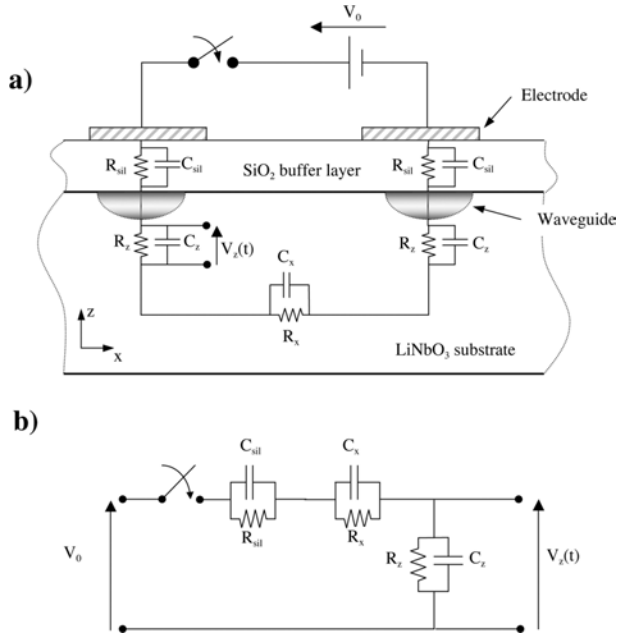

Fig. 2. (a) Equivalent circuit that models the charge storage effects that are due to the buffer layer and the substrate anisotropy in a z-cut $LiNbO_3$ MZ modulator. (b) Simplified circuit.

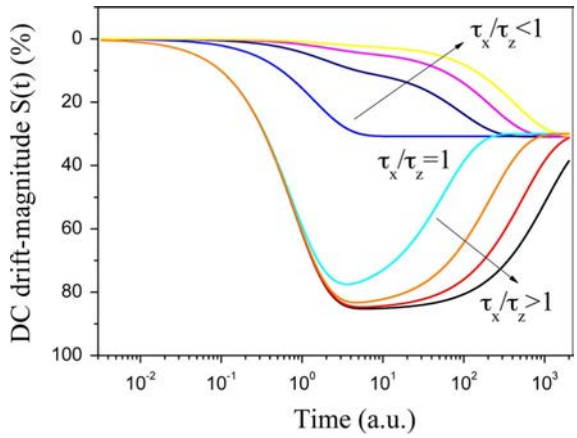

Fig. 3. Role of the substrate anisotropy on the drift magnitude $S(t)$, as deduced from electrical *RC* modelization, in a z-cut $LiNbO_3$ MZ modulator.

of the LN substrate, respectively. Within this model, it is proposed to point out the relative contributions of each layer to the dc drift. Fig. 2(a) shows a typical cross section of a Ti:LN modulator to underline the various material layers that motivate the *RC* model. Each material from which the modulator is constructed is characterized by its own permittivity and conductivity and thus by a proper *RC* circuit. As the asymmetry, of the interferometer or the excitation, does not play any role in the intrinsic drift (asymmetry of the applied voltage only changes the value of the initial applied electric field but does not affect its time dependence and unbalanced interferometer does not induce any change of the amplitude or time dependence of the electric field), a more simple equivalent circuit, as depicted in Fig. 2(b), can be derived, allowing easier calculation. At some instant denoted by $t = 0$, a constant external voltage V_0 is applied to the input terminal of the circuit. To know the behavior of the voltage drops through the waveguide region, we study the time dependence $S(t)$ (1) thanks to the analysis of the circuit drawn in Fig. 2(b), which leads to

$$S(t) = A + Be^{-t/\tau} + Ce^{-t/\tau'} \tag{3}$$

where A, B, C, τ, and τ' are constants depending on the values of the different resistances and capacitances as defined in Fig. 2(b) (see Appendix IV for details). The time dependence of the drift magnitude $S(t)$, calculated according to (3) and using values of physical constant of LN given in Appendix III, is plotted in Fig. 3 for different values of the ratio $(\tau_x)/(\tau_z)$ related to the anisotropy of the LN substrate and for $\tau_{\text{sil}} \ll \tau_x, \tau_z$. $\tau_{\text{sil}}, \tau_x$, and τ_z are the characteristic times of the *RC* circuits associated with the silica buffer and to the LN substrate along the x- and z-axes, respectively (see Appendix IV for details).

We can see that $S(t)$ varies monotonously with time when $\tau_x < \tau_z$, whereas the time dependence is nonmonotonous for $\tau_x > \tau_z$. The shape of the temporal behavior of $S(t)$ is thus strongly correlated with the electrical anisotropy of the LN substrate. Within the steady state, the value of $S(t)$ does not depend on the ratio $(\tau_x)/(\tau_z)$ and is only determined by the resistivity anisotropy ratio $(\rho_x)/(\rho_z + \rho_x)$ of the LN substrate (see Appendix IV).

In the transient regime, the amplitude of the variations of $S(t)$ depends largely on the electrical anisotropy of the LN substrate, and the time dependence of $S(t)$ exhibits a large variation characterized by two response times which differ from more than two orders of magnitude. Fig. 3 shows also that the shortest response time weakly depends on the ratio $(\tau_x)/(\tau_z)$ and is thus mainly related to the electrical characteristics of the silica buffer layer. This correlates the observations of Nagata *et al.* [15] who have shown that the short-term dc drift is affected by the characteristics of the SiO_2 buffer layer, which depends on the SiO_2 deposition method [2], [16]. The largest response time is strongly dependent on the ratio $(\tau_x)/(\tau_z)$ (see Fig. 3) and, as shown in Fig. 4 which shows the relative dependence of the short and long response times of the drift magnitude $S(t)$ as calculated according to (IV.33) and (IV.34), weakly affected by the electrical characteristics of the silica buffer layer.

In the short time range, the amplitude of $S(t)$ is determined by the relative anisotropy of the dielectric permittivity ratio $(\epsilon_z)/(\epsilon_z + \epsilon_x)$ (see Appendix IV). This is in partial contradiction with the observations of Nagata *et al.* [15] who have highlighted a correlation between the magnitude of the short dc drift and the quality of the SiO_2 buffer layer altered by unwanted contaminants such as Na^+ and K^+ ions [17], [18] easily incorporated from the photoresist developers used during the patterning process, Li^+ ions from $LiNbO_3$ substrates, which may diffuse throughout the SiO_2 layer during the heating process, and OH ions adsorbed from room atmosphere [19] in the silica buffer. Nevertheless, as shown below (see Section III-B), this correlation is more probably due to the modification of the LN substrate during the process (out-diffusion of Li^+ ions) than the alteration of the silica buffer.

Therefore, among several different solutions, Kim *et al.* [17] have proposed a technique to remove, using a chemical-cleaning process, all the alkali contaminants (especially Na^+ and K^+

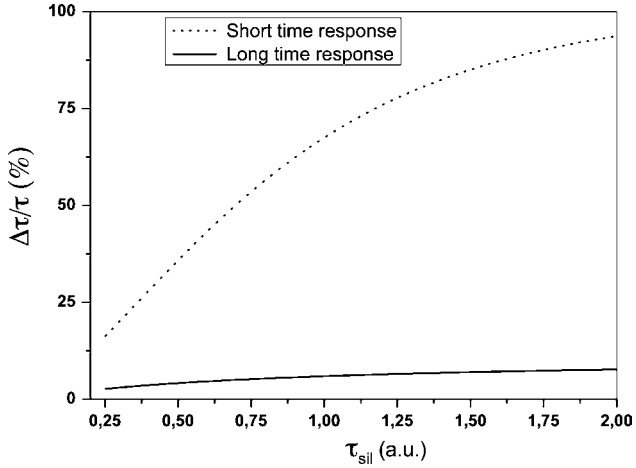

Fig. 4. Relative dependences $(\Delta\tau)/(\tau)$ and $(\Delta\tau')/(\tau')$ of the short τ and long τ' response times of the drift magnitude $S(t)$, respectively, with the electrical characteristic time of the silica buffer layer, as deduced from electrical *RC* modelization, in a z-cut $LiNbO_3$ MZ modulator.

ions) from the buffer layer, and to diminish drastically the OH ions contents with an adapted annealing process. To reduce the mobility of the Li^+ ions, Jin *et al.* [20] have used F^- ions implanted SiO_2 layer. These solutions allow to reduce the short-term drift only.

In contrary, and to our knowledge, very few studies showing the role of the LN substrate anisotropy in the long-term dc drift have been published. One can cite Johnston *et al.* [21] who have proposed to reduce the dielectric relaxation time of the LN substrate by adjusting the bulk electrical resistivity as it was discussed in Appendix II-A.

B. Experimental Approach

In order to get further understanding on the role of the LN substrate anisotropy, we have characterized the dc drift in an LN:Ti MZ modulator. The silica buffered z-cut LN MZ modulator used in this experiment was prepared using common photolithographic and thin-film formation techniques. The waveguide is formed on a z-cut LN wafer along the x-direction by Ti in-diffusion. The drift is measured by the phase-tracking method (see Appendix I-B), as follows. Light delivered by a current and temperature-controlled pigtailed DFB laser diode emitting at 1.55 μm wavelength with low optical power (a few hundreds μW) is fed into the waveguides via a monomode polarization maintaining optical fiber. The modulator is driven by an ac 1 kHz voltage of peak-to-peak value $V_{p-p} = 1.4$ V under constant dc bias during the operation. The optical output is detected using a GaAs p-i-n photodiode followed by a current-to-voltage amplifier, and is recorded using an oscilloscope. The whole setup is placed in a temperature-controlled (± 0.1 °C) chamber.

The thermal and time drifts of the laser diode, photodetector, dc and ac voltage supply, and different measurement apparatus are taken into account during the analysis of the results. The thermal variation of the whole setup (including the MZ modulator), expressed in terms of relative output intensity variation, is equal to 3.4%/K, leading to less than 1% (for several hundreds of hours of operation) of thermal contribution during

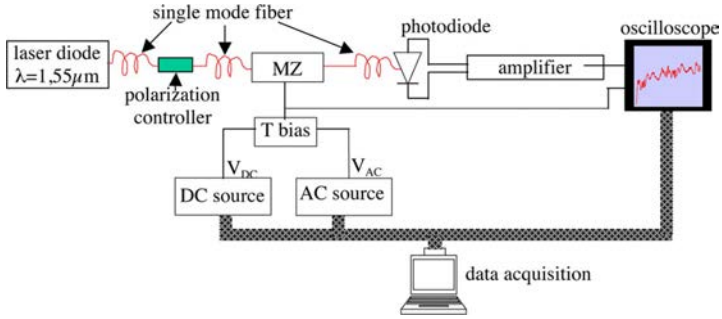

Fig. 5. Schematic of dc drift recording arrangements.

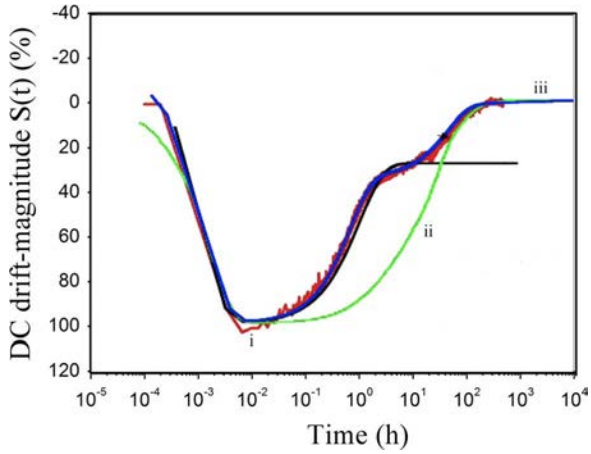

Fig. 6. Typical record of the dc drift in a z-cut $LiNbO_3$ MZ modulator: (i) measurements, (ii) simulation according to the electrical circuit of Fig. 2 and (3), (iii) simulation according to the electrical circuit of Fig. 7 and (4).

the dc drift-magnitude measurements under temperature-controlled environment. The experimental arrangement that we used is shown in Fig. 5. Under these conditions, thermal, photoinduced, and strain-induced drift should not occur. To activate dc drift, a dc bias step voltage of 3.3 V is chosen, allowing to operate the device at the quadrature working point. The drift of the modulator is observed as the time-dependence change of the optical output intensity of the modulator, and expressed by the parameter $S(t)$ as described in Appendix I-B. A typical record of the dc drift is shown in Fig. 6(i). Before reaching its steady-state value, the time dependence of $S(t)$ exhibits a transient characterized by three response times with values equal to a few seconds, a few tens of minutes and a few tens of hours, respectively. Thus, the model based on the circuit in Fig. 2 and the use of (3) to simulate and reproduce the time evolution of $S(t)$ is no longer valid [see Fig. 6(ii)]. The electrical circuit (see Fig. 2) has to be modified by taking into account of additional *RC* elements. We propose to take into account the modification of the top surface of the LN substrate in the waveguide region which can be affected by the fabrication process of the waveguides (Ti in-diffusion in our case). More especially, modifications of the local electrical conductivity can occur during the high-temperature process required for the Ti in-diffusion. Since chemical reduction gives additional electrons trapped at niobium sites, the chemical reduction reaction at the top surface can thus lead to local electrical conductivity gradients. For this, and as shown in

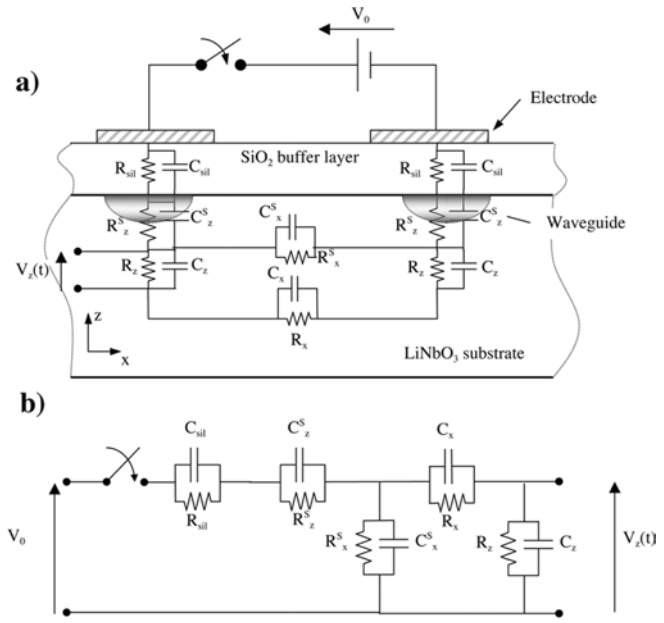

Fig. 7. (a) Equivalent circuit that models the charge storage effects that are due to the buffer layer, the substrate anisotropy, and inhomogeneity in a z-cut $LiNbO_3$ MZ modulator. (b) Simplified circuit.

Fig. 7, two more *RC* circuits, should be added in the model, leading to a new expression of the drift magnitude $S(t)$ as

$$S(t) = D + Ee^{-t/\tau_d} + Fe^{-t/\tau'_d} + Ge^{-t/\tau''_d} \tag{4}$$

where $D, E, F, G, \tau_d, \tau'_d$, and τ''_d are constants depending on the values of the different resistances and capacitances of the new electrical circuit. The corresponding curve is plotted in Fig. 6(iii) using values of τ_d, τ''_d, and τ'_d equal to 4 s, 40 mn, and 60 h, respectively. As described earlier, the shortest τ_d and longest τ'_d response times can be attributed to charge relaxations in the silica buffer layer and the LN substrate, respectively. The third response time τ''_d is linked to charge relaxation at the top surface of the LN substrate in the waveguide region (described by the new *RC* circuits).

The calculation of the different response times via the model, described in Fig. 7, leads to rather complicated and heavy expressions. Moreover, the evaluation of the values of $R^S_{x,z}$ and $C^S_{x,z}$ is quite difficult since they correspond to modifications of the LN properties, due to the Ti in-diffusion process for the realization of the waveguides, which are not known. Nevertheless, it is possible to establish the relation between the two response times τ'_d and τ''_d. The analysis of electrical circuits, such as this presented in Fig. 2, leads to a ratio of the large and short response times of $S(t)$ proportional to the ratio of the two larger characteristic times associated with the different *RC* circuits. Then, according to Fig. 7, we can write

$$\begin{aligned} \frac{\tau'_d}{\tau_d} &\propto \frac{\tau_x}{\tau_z} = \frac{R_x C_x}{R_z C_z} \\ \frac{\tau''_d}{\tau_d} &\propto \frac{\tau^S_x}{\tau^S_z} = \frac{R^S_x C^S_x}{R^S_z C^S_z}. \end{aligned} \tag{5}$$

If we assume that the dielectric permittivities of the LN substrate are not modified by the technological process ($C^S_z \approx C_z$ and $C^S_x \approx C_x$), and that the modification of the electrical conductivity can be described by

$$\begin{aligned} R^S_x &= R_x + \Delta R_x \\ R^S_z &= R_z + \Delta R_z \end{aligned} \tag{6}$$

then we have

$$\frac{\tau'_d}{\tau''_d} = \frac{R_z R^S_x}{R^S_z R_x} = \frac{1 + (\Delta R_x)/R_x}{1 + (\Delta R_z)/R_z} \approx \frac{(\Delta R_x)/R_x}{(\Delta R_z)/R_z} \tag{7}$$

in the case of large variations, induced during the technological process, of the electrical conductivity in the waveguide region of the LN substrate. According to (6), it is easy to show that

$$\begin{aligned} \frac{\partial}{\partial x}\frac{\Delta R_x}{R_x} &= \left(\frac{\partial}{\partial x}\left(\frac{\Delta\sigma_x}{\sigma_x(x=x_0)}\right)\right)^{-1} \\ \frac{\partial}{\partial z}\frac{\Delta R_z}{R_z} &= \left(\frac{\partial}{\partial z}\left(\frac{\Delta\sigma_z}{\sigma_z(z=0)}\right)\right)^{-1} \end{aligned} \tag{8}$$

where $\sigma_x(x = x_0)$ and $\sigma_z(z = 0)$ are the conductivities at the border of the waveguide along *X*- and *Z*-axes (see Figs. 8 and 9), respectively. $\Delta\sigma_x = \sigma_x(x = 0) - \sigma_x(x = x_0)$ and $\Delta\sigma_z = \sigma_z(z = 0) - \sigma_z(z = z_0)$ are the conductivities variations over the waveguide. Thus, (8) becomes

$$\begin{aligned} \frac{\Delta R_x}{R_x} &= \left(\frac{\Delta\sigma_x}{\sigma_x(x=x_0)}\right)^{-1} \\ \frac{\Delta R_z}{R_z} &= \left(\frac{\Delta\sigma_z}{\sigma_z(z=0)}\right)^{-1}. \end{aligned} \tag{9}$$

If we assume that

$$\begin{aligned} \Delta\sigma_x &\sim \frac{\partial\sigma_x}{\partial x} x_0 \\ \Delta\sigma_z &\sim \frac{\partial\sigma_z}{\partial z} z_0 \end{aligned} \tag{10}$$

where x_0 and z_0 are the dimensions of the waveguide along *X*- and *Z*-axes, respectively, then (9) becomes

$$\begin{aligned} \frac{\Delta R_x}{R_x} &\sim \left(\frac{1}{\sigma_x(x=x_0)}\frac{\partial\sigma_x}{\partial x}\right)^{-1} x_0 \\ \frac{\Delta R_z}{R_z} &\sim \left(\frac{1}{\sigma_z(z=0)}\frac{\partial\sigma_z}{\partial z}\right)^{-1} z_0 \end{aligned} \tag{11}$$

where $(1)/(\sigma_x(x = x_0))(\partial\sigma_x)/(\partial x)$ and $(1)/(\sigma_z(z = 0))(\partial\sigma_z)/(\partial z)$ are the relative conductivity gradients along *X*- and *Z*-axes, respectively. They have been evidenced by our group, by means of a polaron microphotoluminescence technique [22]. We have shown that the polaron luminescence is a sensitive probe to measure the chemical reduction in LN. The photoluminescence signal $I^{x,z}_{\mathrm{PL}}$ recorded point by point in the cross section of the waveguide allows to obtain the profiles of the relative chemical reduction at the top surface. The latter leads to the corresponding profiles of $\sigma_{x,z}$, since chemical reduction reaction gives additional

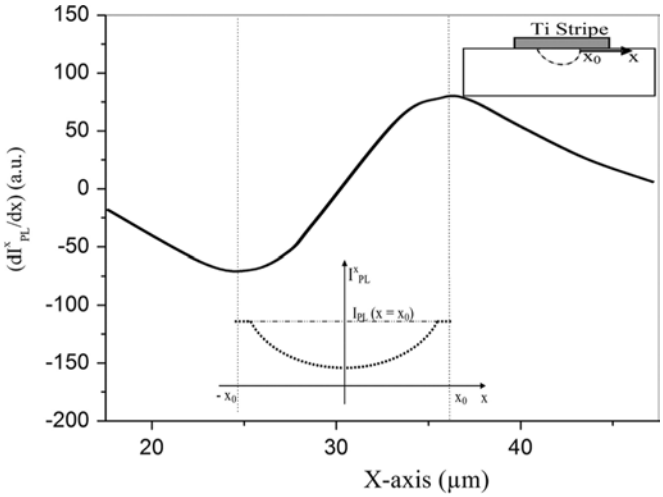

Fig. 8. Relative photoluminescence profile along *X*-direction in a *z*-cut $LiNbO_3$ MZ modulator [22].

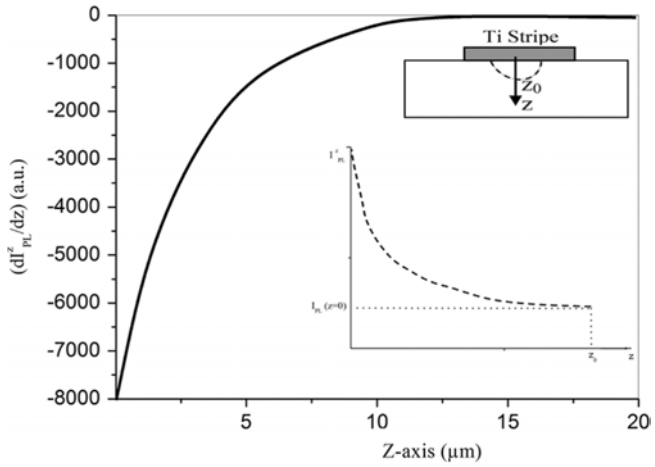

Fig. 9. Relative photoluminescence profile along *Z*-direction in a *z*-cut $LiNbO_3$ MZ modulator [22].

electrons trapped at niobium sites that modify the local conductivity. Thus, (11) becomes

$$\frac{\Delta R_x}{R_x} \sim \left(\frac{1}{I_{\rm PL}(x=x_0)}\frac{\partial I^x_{\rm PL}}{\partial x}\right)^{-1} x_0$$
$$\frac{\Delta R_z}{R_z} \sim \left(\frac{1}{I_{\rm PL}(z=0)}\frac{\partial I^z_{\rm PL}}{\partial z}\right)^{-1} z_0 \qquad (12)$$

where

$$(1)/(I_{\rm PL}(x=x_0))(\partial I^x_{\rm PL})/(\partial x)$$

and

$$(1)/(I_{\rm PL}(z=0))(\partial I^z_{\rm PL})/(\partial z)$$

are the derivatives of the polaron luminescence signal along *X*- and *Z*- axes, respectively. Equation (7) can be finally written as

$$\frac{\tau'_d}{\tau''_d} \approx \frac{\partial/\partial z\,(\sigma_z/\sigma_z(z=0))}{\partial/\partial x\,(\sigma_x/\sigma_x(x=x_0))}\frac{z_0}{x_0}$$
$$\approx \frac{\partial/\partial z\,(I^z_{\rm PL}/I_{\rm PL}(z=0))}{\partial/\partial x\,(I^x_{\rm PL}/I_{\rm PL}(x=x_0))}\frac{z_0}{x_0}. \qquad (13)$$

The photoluminescence signals were measured on Ti in-diffused waveguides that were fabricated using the same technological process as commercial LN MZ modulators, along *X*- and *Y*-axes. Along the *X*-axis, the chemical reduction, and thus the photoluminescence signal $I^x_{\rm PL}$ increases across the waveguide region, reaches a maximum at the middle of the waveguide and then decreases, leading to the curve plotted on Fig. 8 for its derivative. Along *Z*-axis, the chemical reduction, and thus the photoluminescence signal $I^z_{\rm PL}$ decreases monotonically, leading to the curve plotted on Fig. 9 for its derivative. Using (13) and data of Figs. 8 and 9 leads to a value of $(\tau')/(\tau'')$ equal to about 100 (the dimension x_0 and z_0 of the waveguide are nearly equal). The value of $(\tau')/(\tau'')$ as deduced from the data in Fig. 6(iii) is found to be equal to 90, corroborating our interpretation.

IV. Proposed Solution

Our approach consists of the control of the inhomogeneities in the electrical conductivity, which appear in the waveguide region of the MZ modulator and due the fabrication process of the latter. An appropriate engineering of these inhomogeneities should allow to obtain a charge relaxation at the top surface of the LN substrate which could exactly compensate the charge relaxation in the bulk LN substrate. Doing this, the long-time dc drift would be eliminated and only the short-time dc drift, induced by charge relaxation in the silica buffer, would remain. This is not really a problem since the startup time of the system is larger than this short-time dc drift which is equal to a few seconds.

According to (2), the electrical stability can be obtained if

$$\text{div}\,[\epsilon]\vec{E} = 0, \quad \text{div}\,[\sigma]\vec{E} = 0. \qquad (14)$$

We assume that the chemical reduction does not affect the dielectric permittivities and that the modifications of the electrical conductivities are isotropic. Thus, we can consider that the ratio of electrical conductivities $(\sigma_x)/(\sigma_z)$ and dielectric permittivities ϵ_x and ϵ_z are constant for all (x,z) points in the LN substrate. Equation (14) becomes

$$\frac{\epsilon_x E_x}{\epsilon_z E_z}\frac{\partial \ln \sigma_z}{\partial x} + \frac{\tau_x}{\tau_z}\frac{\partial \ln \sigma_z}{\partial z} = \left(1 - \frac{\tau_x}{\tau_z}\right)\frac{\partial \ln E_z}{\partial z}. \qquad (15)$$

Solving this equation leads to the determination of the electrical conductivity profiles, along *x*- and *z*-axes, or the ideal electrical conductivity map, which allow to obtain a stable (no time evolution) electric field in the waveguides region. The calculation of this ideal conductivity map requires the knowledge of the:

- electric field profile in the waveguides region;
- initial electrical conductivity map at the top surface of the LN substrate;
- τ_x and τ_z values for the chosen LN substrate.

The electric profile can be determined by numerical calculation and can be achieved from several existing numerical tools using finite element method. As we have seen earlier, the determination of the initial electrical conductivity map can be obtained using the microphotoluminescence technique. Finally, the two

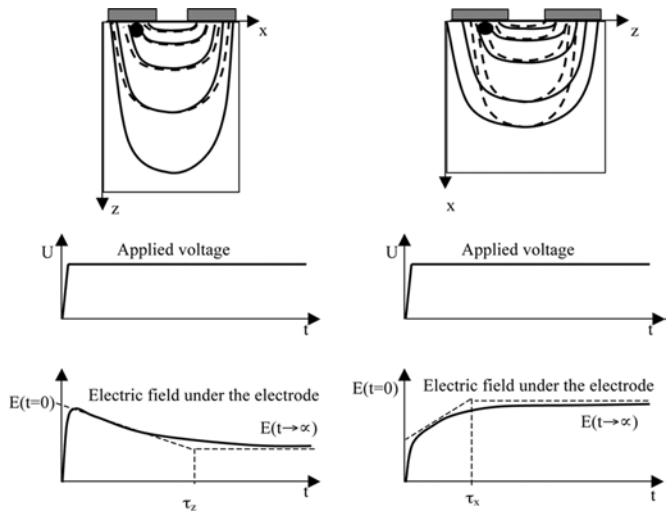

Fig. 10. Samples and technique for the derivation of the values of the characteristic times τ_x and τ_z. The circle indicates the light-beam.

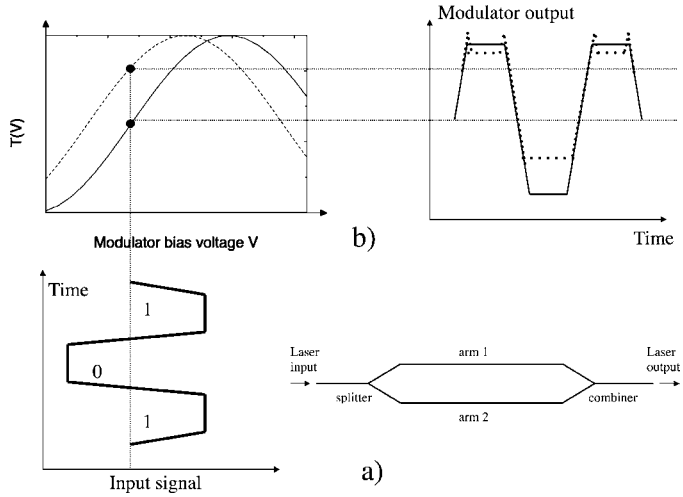

Fig. 11. Schematic drawing of an MZ transfer function. The drift phenomenon and the associated signal distortion which may occur is illustrated.

characteristic times τ_x and τ_z can be derived from the record of the time evolution of the phase shift induced by a dc voltage in *x*-cut and *z*-cut LN substrates on which coplanar electrodes have been deposited (see Fig. 10). This can be realized using a simple optical technique, as it was shown by Twu *et al.* [23].

V. Conclusion

In this paper, we have discussed and analyzed the different sources of the drift in commercially available LN MZ modulators. The different origins have been compared in terms of phase shift and the different corresponding orders of magnitude have been given, pointing out the predominant role of the dc drift. We have then shown the large role played by the electrical inhomogeneities at the surface of the LN substrate by highlighting the link between the time dependence of the dc drift in an LN MZ modulator and the electrical conductivity measured at the surface and in the volume of the LN substrate. Finally, we have proposed a solution to the issue of the intrinsic (or dc) drift, consisting in the electrical engineering of the electrical conductivity of the LN substrate surface in order to suppress the long-term dc drift. The study, with the goal to calculate and realize the ideal conductivity map on simple waveguide devices in a first step, is still in progress and will be presented in a next paper.

Appendix A
MZI Modulators: Characteristics and Measurements Techniques of the Drift

A. Characteristics of the MZ Modulators

The MZ interferometer is based on the electro-optic (EO) effect. Fig. 11(a) shows a schematic drawing of such an interferometer. At its optical input port, there is an optical splitter that divides the input optical beam into two equal beams. The divided beams propagate in two separate arms. At least one of these arms is designed [24] as an EO waveguide, along which the optical phase can be modulated by an applied voltage.

If the optical waves are in phase after propagating through the two arms, they combine as a single mode in the output optical combiner, which results in a maximum intensity output; whereas if the optical waves are out of phase after propagating through the two arms, they combine as a higher order spatial mode near the optical combiner, therefore most of the optical power becomes an unguided wave beyond the combiner and the output intensity is a minimum. The optical field amplitude at the output of the MZ modulator can be generally represented by

$$A_{\text{out}} = \frac{\sqrt{2}}{2}\left(A_1 e^{j\Phi_1} + A_2 e^{j\Phi_2}\right) \tag{I.16}$$

where A_1 and A_2 correspond to the optical amplitudes in the two arms, and Φ_1 and Φ_2 represent the optical phase delays. The optical intensity transmission (or transfer function), which corresponds to the ratio of the optical output power to the optical input power can be written in the form of

$$T = \frac{1}{2}(1 + b\cos(\Phi_1 - \Phi_2)) \tag{I.17}$$

where $b = 2A_1A_2/(A_1^2 + A_2^2)$ is an optical imbalance factor between the two arms, and $b = 1$ for ideally balanced design. Optical losses at the device facets and during propagation are ignored in the previous derivation. The phase difference $\Phi_1 - \Phi_2$ consists of two parts: one is the phase difference Φ_0 at zero applied voltage; the other is the phase difference $\Delta\Phi$ due to the applied voltage. When only one arm is modulated, the phase difference becomes

$$\Delta\Phi = \gamma\Delta n\frac{2\pi}{\lambda}L \tag{I.18}$$

where γ is the optical confinement factor, defined as the portion of optical mode that is confined in the active layer; λ is the optical wavelength; L is the modulation length; Δn is the optical index change in the waveguide active layer

$$\Delta n = \frac{1}{2}n_{\text{eff}}^3 r_{\text{eff}}\frac{V}{d} \tag{I.19}$$

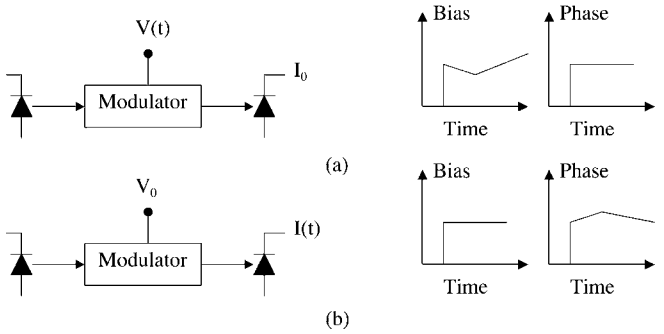

Fig. 12. Schematics of stability testing arrangements: (a) constant internal voltage (null-tracking measurement) and (b) constant external voltage (phase-tracking measurement).

where n_{eff} is the effective optical index of the active layer at zero applied voltage; r_{eff} is the effective EO coefficient, determined by the material, optical polarization, and electrode design [24]. *V* is the applied voltage; d is the spatial gap between the electrodes across which the voltage *V* is applied. Combining (I.18) and (I.19), (I.17) can be written as

$$T(V) = \frac{1}{2}\left(1 + b\cos\left(\pi\frac{V}{V_\pi} + \Phi_0\right)\right) \tag{I.20}$$

V_π is the half-wave voltage value corresponding to an induced phase difference equal to π and defined by

$$V_\pi = \frac{\lambda}{n_{\text{eff}}^3 r_{\text{eff}}}\frac{d}{\gamma L}. \tag{I.21}$$

A typical transfer function $T(V)$, described by (I.20), as well as the output modulation signal for an MZ modulator is shown in Fig. 11(b). The drift phenomenon and the associated signal distortion which may occur are also illustrated.

Packaged LN MZ modulators are mainly composed of a titanium-diffused or proton-exchanged waveguide, a rf-port section (for the modulating voltage V) with a silica buffer layer, a separate dc bias port with or without a buffer layer, and electroplated gold electrodes. Typical device fabrication procedures have been reported elsewhere [24]–[26].

B. Measurement Techniques of the Drift

Two methods [3] are commonly used to assess the bias stability of LN EO devices. These are illustrated schematically in Fig. 12. In one method, Fig. 12(a), the bias voltage, which is initially at zero potential, is rapidly changed to a value chosen to set the device in a unique optical state, which is characterized by a value of the optical phase. Following this, the applied voltage is continuously adjusted to maintain this state. The selected bias voltage may correspond to the optical state of maximum extinction (i.e., a null), maximum transmission, or maximum linearity.

In the second method [see Fig. 12(b)], the modulator bias is rapidly increased from zero to a predetermined level. The applied voltage is then held constant at this value and the output of the modulator is continuously monitored to determine the electro-optically induced optical phase shift as a function of time.

The changing optical phase shift may be expressed in terms of a drift magnitude parameter S corresponding to an effective voltage shift $\Delta V(t)$ at time *t*, since for the linear EO effect the internal phase shift is proportional to a measurable external voltage, normalized to the initial applied voltage transient $V_m(0)$

$$S = \frac{\Delta V(t)}{V_m(0)}. \tag{I.22}$$

The relative voltage shift $\Delta V(t)$ at time *t* is given by

$$\Delta V = V_m(t) - V_m(0). \tag{I.23}$$

For a value of $V_m(0)$ equal to the quadrature bias voltage $V_m(0) = (V_\pi)/(2)$, and using (I.18), (I.19), and (I.21), (I.22) becomes

$$S = \frac{\Delta V}{V_\pi/2} = \frac{2\Delta\Phi}{\pi} \tag{I.24}$$

where $\Delta\Phi$ is defined by (I.18).

II. Different Extrinsic Sources of Drift

In the following, we propose to classify and describe more in detail the different possible sources of the drift in LN MZ modulators, and the technical solutions used to suppress or at least reduce the drift issue. The extrinsic origins of the drift are linked to the change of the effective refractive index of the optical mode of the waveguide via the possible variations of the temperature of the device (thermo-optic and pyroelectric effects), of the optical power in the waveguide (photorefractive effect) and the strain relaxation at the silica buffer-substrate interface (strain-optic effect). Here, we summarize and analyze the different origins from the studies reported in the literature.

A. Thermal Drift

The thermal drift originates from both thermo-optic and pyroelectric properties of the titanium-diffused or proton-exchanged LN waveguides. The thermo-optic effect gives rise to a change of the effective refractive index of the material. Since LN crystal is ferroelectric and pyroelectric, the temperature change experienced by the LN substrate results in a variation of the spontaneous polarization leading to the creation of a transient depolarizing electric field and then to an additional refractive index change. The corresponding unwanted phase shifts, which superimpose to those induced by the bias voltage yields a drift of the bias point in the case of a temperature change of the device. The thermal drift, as recorded by Nagata and Ichikawa [2], is quite complex. This is expected since, in contrary to the thermo-optic effect, the pyroelectric effect induces transient contribution to the drift. Moreover, the measurement technique, for which the bias voltage is not constant, contributes to this complexity since this method certainly induces intrinsic drift.

Several solutions have been proposed and used to suppress, or strongly reduce [27] these thermal drift sources. The thermal drift can occur only in the case of asymmetric MZ modulator (refractive index inhomogeneities) or if the temperature variation experienced by each of the arms is different (see Table II). If the optical lengths of the two arms of the interferometer are equal, the phase shifts induced by an homogeneous temperature

change in both arms are equal and the bias point is stable. For symmetric MZ modulators, thermal drift can exist only if the temperature variation in each arm is different. These two technological point seem to be well controlled [27]. For instance, a charge-bleed layer is applied to suppress the pyroelectric-dominated thermal shift [28], [29]. Shafer *et al.* [30] have proposed to apply conductive paint or conductive epoxy to the sides of the LN substrate. In the same way, the authors also showed that a metallisation on the $+z$ and $-z$ surfaces (the sides) of the substrate and the use of conductive feet to electrically connect the $+z$ and $-z$ surfaces can be a solution to suppress the thermal shift due to pyroelectric effect. Johnston *et al.* [21] have proposed to use a device where the bulk resistivity of at least a portion of the substrate is no greater than 10^{13} Ω·cm. The reduction in bulk resistivity reduces the dielectric relaxation time of the substrate crystal and, therefore, does not allow substantial charge to be accumulated at the surfaces due to the pyroelectric effect.

B. Photoinduced Drift

Under high-intensity optical radiation, LN is known to change its refractive index. The photorefractive process results from the combination of electro-optic, photovoltaïc, and photoconductive properties of the material. In the MZ interferometer, light is balanced equally in two arms, so that the index differences due to the photovoltaïc effect will be of equal sign and magnitude in the two arms of the device. Since the output of the device depends on the phase difference between the arms, no change will occur from photovoltaïc phenomena unless index inhomogeneities or intensity differences between waveguides. The MZ modulator is also affected by the photoconductive process. The higher region of photoconductivity partially screens out the field in the region of the waveguide. This screening changes the bias point of the device due to the buildup of an internal space charge field. Photorefractive effect is known to be large at short (less than 830 nm) wavelengths in $LiNbO_3$ [31]. Betts *et al.* [32] have reported large photoinduced bias drift in *x*-cut titanium-diffused waveguide devices, at 1064 nm and at 90 mW of optical power, but also at 1320 nm at 130 mW.

As a solution, the authors of [32] have shown that the sensitivity of the drift to photorefractive effect is largely reduced by an anneal in wet oxygen. The explanation is that the anneal process decreases the $(Fe^{2+})/(Fe^{3+})$ ratio from one part, and from the other part, that positively charged ions (H^{+}) can move to compensate the electric field produced by the photorefractive effect. The thermal fixing method for reducing photorefractive sensitivity [33] takes advantage of this.

C. Strain-Induced Drift

In high-speed applications of LN MZ modulators, the thicknesses of the silica buffer layer and the gold electrodes are required to be as large as micrometers for impedance and velocity matching. Such thick overlayers cause a deformation of the LN substrate, resulting in possible fluctuations of the refractive index of the waveguide via the piezo-optical effect [34]. The internal stress in the film is reported to depend on the deposition method and its parameters. In general, buffer layers with greater density for the purpose of improved stability tend to exhibit higher internal stresses which deform the substrate. In such mechanically strained modulators, optical phase shifts can be induced by deformation recovery, strain relaxation due to biasing, and temperature variations (large difference of thermal expansion coefficients between $LiNbO_3$ and SiO_2). As for the other sources of extrinsic drift, the strain-induced drift can occur only if the interferometer is unbalanced or if the strain relaxation is different from one arm to the other.

To overcome this problem, Nagata *et al.* [16] have proposed the deposition, on the opposite (bottom) surface of the LN substrate, of a supplementary silica layer. The role of this latter layer is to counterbalance the deformation induced by the silica buffer layer deposited on the top surface of the substrate. In that way, the authors have shown that a 1.3 μm thick silica film deposited at the bottom surface of the LN surface reduces the LN substrate deformation (deflection) induced by a 1.3 μm silica buffer layer deposited at the top surface, from 32 μm down to 8 μm.

III. Used Values of Physical Parameters of $LiNbO_3$ and SiO_2

The different values of the physical parameters of $LiNbO_3$ and SiO_2 used in this paper are given in Table IV.

IV. Expression of the Parameters A, B, τ, and τ' Involved in the Drift Magnitude S

The voltage $V_z(t)$ (see Fig. 2) can be easily expressed in terms of electrical impedances as shown in the equation (IV.25) of the page, where $p = j\omega$ and $(V_0)/(p)$ is the applied voltage. Using the inverse Laplace transform, (IV.25) becomes

$$\begin{aligned}\frac{V_z(t)}{V_0} = \frac{R_z}{a} + e^{-\frac{1}{2}\frac{b}{2c}t} \\ \times \left\{ \left[-\frac{b}{2c}\frac{R_z}{a}\frac{1}{\omega} + \frac{R_z R_{\mathrm{sil}} C_{\mathrm{sil}} + R_z R_x C_x}{c} \right.\right. \\ \left. -\frac{b}{2c^2\omega} R_{\mathrm{sil}} R_z R_x C_{\mathrm{sil}} C_x \right] \sin h(\omega t) \\ \left. + \left[-\frac{R_z}{a} + \frac{R_{\mathrm{sil}} R_z R_x C_{\mathrm{sil}} C_x}{c} \right] \cos h(\omega t) \right\}\end{aligned} \tag{IV.26}$$

$$V_z(p) = \frac{R_z/(1+R_z C_z p)}{R_{\mathrm{sil}}/(1+R_{\mathrm{sil}} C_{\mathrm{sil}} p) + R_z/(1+R_z C_z p) + R_x/(1+R_x C_x p)} \frac{V_0}{p} \tag{IV.25}$$

TABLE IV
USED VALUES OF PHYSICAL PARAMETERS OF $LiNbO_3$ AND SiO_2. σ IS THE ELECTRICAL CONDUCTIVITY, ϵ_{LF} IS THE LOW-FREQUENCY DIELECTRIC PERMITTIVITY, N IS THE REFRACTIVE INDEX, $\beta, (dn)/(dT), (dP_s)/(dT), r$, AND p ARE, RESPECTIVELY, THE PHOTOVOLTAIC, PYROELECTRIC, THERMO-OPTIC, ELECTRO-OPTIC, AND ELASTO-OPTIC COEFFICIENTS

	n	ϵ_{LF}	β (GV^{-1})	σ ($\Omega^{-1}m^{-1}$)	$\frac{dn}{dT}$ (K^{-1})	$\frac{dP_s}{dT}$ ($Cb\ cm^{-2}K^{-1}$)	r ($pm\ V^{-1}$)	p
$LiNbO_3$	2.14 [35]	ϵ_z = 35 [36] ϵ_x = 95 [36]	β_{33} = 4.2 [37]	$\approx 10^{-19}$ [38]	4.41 10^{-5} [39]	-6.4 10^{-9} [40]	31 [41]	0.17 [42]
SiO_2	1.43 [19]	3.9 [43]	-	$\approx 10^{-12}$ [43]	-	-	-	-

with a, b, c, and ω equal to

$$\begin{aligned} a &= R_{\text{sil}} + R_z + R_x \\ b &= R_{\text{sil}}(\tau_x + \tau_z) + R_z(\tau_x + \tau_{\text{sil}}) + R_x(\tau_{\text{sil}} + \tau_z) \\ c &= R_{\text{sil}}\tau_x\tau_z + R_z\tau_x\tau_{\text{sil}} + R_x\tau_{\text{sil}}\tau_z \\ \omega &= \left(\left(\frac{b}{2c}\right)^2 - \frac{a}{c}\right)^{1/2} \end{aligned} \tag{IV.27}$$

where τ_x, τ_z, and τ_{sil} are the characteristic times related to the $LiNbO_3$ substrate and silica buffer layer, respectively. They are defined by

$$\begin{aligned} \tau_x &= R_x C_x \\ \tau_z &= R_z C_z \\ \tau_{\text{sil}} &= R_{\text{sil}} C_{\text{sil}}. \end{aligned} \tag{IV.28}$$

Thus, the drift magnitude can be written as

$$S(t) = A + Be^{-t/\tau} + Ce^{-t/\tau'} \tag{IV.29}$$

where A, B, C τ, τ' are given by the equations at the bottom of the page.

The resistances corresponding to the LN substrate are much larger than the one associated with the silica buffer (the resistivity of LN crystal is much larger than the one of silica). On contrary, due to its small thickness, the capacitance corresponding to the silica buffer, is much larger than those associated with the LN substrate. Thus, as shown by (IV.37)

$$\begin{aligned} &S(t \longrightarrow \infty) \\ &\quad = -\frac{\tau_5 + \tau_{\text{sil}}}{\tau_{\text{sil}} + \tau_4 + \tau_5} \\ &\quad = -\frac{R_{\text{sil}} + R_x}{R_{\text{sil}} + R_z + R_x} \approx -\frac{R_x}{R_z + R_x} \\ &S(t \longrightarrow 0) \\ &\quad = -\frac{\tau_z\tau_x + \tau_5\tau_z}{\tau_z\tau_x + \tau_4\tau_x + \tau_5\tau_z} \\ &\quad = -\frac{\frac{1}{C_x} + \frac{1}{C_{\text{sil}}}}{\frac{1}{C_z} + \frac{1}{C_x} + \frac{1}{C_{\text{sil}}}} \approx -\frac{C_z}{C_z + C_x} \end{aligned} \tag{IV.37}$$

$$A = \frac{\tau_{\text{sil}} + \tau_5}{\tau_{\text{sil}} + \tau_4 + \tau_5} \tag{IV.30}$$

$$\begin{aligned} B = \Bigg\{ &-\frac{\tau_{\text{sil}}(\tau_4+\tau_5) + \tau_z(\tau_{\text{sil}}+\tau_5) + \tau_x(\tau_{\text{sil}}+\tau_4)}{2(\tau_{\text{sil}}\tau_z\tau_x + \tau_4\tau_{\text{sil}}\tau_x + \tau_5\tau_{\text{sil}}\tau_z)} \ \frac{\tau_4}{\tau_{\text{sil}}+\tau_4+\tau_5}\frac{1}{\Omega} + \frac{\tau_4}{\tau_{\text{sil}}\tau_z\tau_x + \tau_4\tau_{\text{sil}}\tau_x + \tau_5\tau_{\text{sil}}\tau_z}\frac{\tau_{\text{sil}}+\tau_x}{\Omega} \\ &-\frac{\tau_{\text{sil}}(\tau_4+\tau_5) + \tau_z(\tau_{\text{sil}}+\tau_5) + \tau_x(\tau_{\text{sil}}+\tau_4)}{2(\tau_{\text{sil}}\tau_z\tau_x + \tau_4\tau_{\text{sil}}\tau_x + \tau_5\tau_{\text{sil}}\tau_z)^2}\frac{\tau_4\tau_{\text{sil}}\tau_x}{\Omega} \ -\frac{\tau_4}{\tau_{\text{sil}}+\tau_4+\tau_5} + \frac{\tau_4\tau_{\text{sil}}\tau_x}{\tau_{\text{sil}}\tau_z\tau_x + \tau_4\tau_{\text{sil}}\tau_x + \tau_5\tau_{\text{sil}}\tau_z} \Bigg\} \end{aligned} \tag{IV.31}$$

$$\begin{aligned} C = \Bigg\{ &-\frac{\tau_4}{\tau_{\text{sil}}+\tau_4+\tau_5} + \frac{\tau_4\tau_{\text{sil}}\tau_x}{\tau_{\text{sil}}\tau_z\tau_x + \tau_4\tau_{\text{sil}}\tau_x + \tau_5\tau_{\text{sil}}\tau_z} + \frac{\tau_{\text{sil}}(\tau_4+\tau_5) + \tau_z(\tau_{\text{sil}}+\tau_5) + \tau_x(\tau_{\text{sil}}+\tau_4)}{2(\tau_{\text{sil}}\tau_z\tau_x + \tau_4\tau_{\text{sil}}\tau_x + \tau_5\tau_{\text{sil}}\tau_z)} \times \frac{\tau_4}{\tau_{\text{sil}}+\tau_4+\tau_5}\frac{1}{\Omega} \\ &-\frac{\tau_4}{\tau_{\text{sil}}\tau_z\tau_x + \tau_4\tau_{\text{sil}}\tau_x + \tau_5\tau_{\text{sil}}\tau_z}\frac{\tau_{\text{sil}}+\tau_x}{\Omega} + \frac{\tau_{\text{sil}}(\tau_4+\tau_5) + \tau_z(\tau_{\text{sil}}+\tau_5) + \tau_x(\tau_{\text{sil}}+\tau_4)}{2(\tau_{\text{sil}}\tau_z\tau_x + \tau_4\tau_{\text{sil}}\tau_x + \tau_5\tau_{\text{sil}}\tau_z)^2} \times \frac{\tau_4\tau_{\text{sil}}\tau_x}{\Omega} \Bigg\} \end{aligned} \tag{IV.32}$$

$$\begin{aligned} \tau = \Bigg\{ &\Bigg[-\frac{\tau_{\text{sil}}+\tau_4+\tau_5}{\tau_{\text{sil}}\tau_z\tau_x + \tau_4\tau_{\text{sil}}\tau_x + \tau_5\tau_{\text{sil}}\tau_z} \\ &+\frac{1}{4}\left\{\frac{\tau_{\text{sil}}(\tau_4+\tau_5) + \tau_z(\tau_{\text{sil}}+\tau_5) + \tau_x(\tau_{\text{sil}}+\tau_4)}{2(\tau_{\text{sil}}\tau_z\tau_x + \tau_4\tau_{\text{sil}}\tau_x + \tau_5\tau_{\text{sil}}\tau_z)}\right\}^2 \Bigg]^{\frac{1}{2}} + \frac{\tau_{\text{sil}}(\tau_4+\tau_5) + \tau_z(\tau_{\text{sil}}+\tau_5) + \tau_x(\tau_{\text{sil}}+\tau_4)}{\tau_{\text{sil}}\tau_z\tau_x + \tau_4\tau_{\text{sil}}\tau_x + \tau_5\tau_{\text{sil}}\tau_z} \Bigg\}^{-1} \end{aligned} \tag{IV.33}$$

$$\begin{aligned} \tau' = \Bigg\{ &\Bigg[\frac{\tau_{\text{sil}}+\tau_4+\tau_5}{\tau_{\text{sil}}\tau_z\tau_x + \tau_4\tau_{\text{sil}}\tau_x + \tau_5\tau_{\text{sil}}\tau_z} \ -\frac{1}{4}\left\{\frac{\tau_{\text{sil}}(\tau_4+\tau_5) + \tau_z(\tau_{\text{sil}}+\tau_5) + \tau_x(\tau_{\text{sil}}+\tau_4)}{2(\tau_{\text{sil}}\tau_z\tau_x + \tau_4\tau_{\text{sil}}\tau_x + \tau_5\tau_{\text{sil}}\tau_z)}\right\}^2 \Bigg]^{\frac{1}{2}} \\ &+\frac{\tau_{\text{sil}}(\tau_4+\tau_5) + \tau_z(\tau_{\text{sil}}+\tau_5) + \tau_x(\tau_{\text{sil}}+\tau_4)}{\tau_{\text{sil}}\tau_z\tau_x + \tau_4\tau_{\text{sil}}\tau_x + \tau_5\tau_{\text{sil}}\tau_z} \Bigg\}^{-1}. \end{aligned} \tag{IV.34}$$

$$\begin{aligned} \tau_4 &= R_z C_{\text{sil}} \\ \tau_5 &= R_x C_{\text{sil}} \end{aligned} \tag{IV.35}$$

$$\Omega = \left[\frac{\tau_{\text{sil}} + \tau_4 + \tau_5}{\tau_{\text{sil}}\tau_z\tau_x + \tau_4\tau_{\text{sil}}\tau_x + \tau_5\tau_{\text{sil}}\tau_z} - \frac{1}{4} \left\{ \frac{\tau_{\text{sil}}(\tau_4 + \tau_5) + \tau_z(\tau_{\text{sil}} + \tau_5) + \tau_x(\tau_{\text{sil}} + \tau_4)}{2(\tau_{\text{sil}}\tau_z\tau_x + \tau_4\tau_{\text{sil}}\tau_x + \tau_5\tau_{\text{sil}}\tau_z)} \right\}^2 \right]^{\frac{1}{2}}. \quad \text{(IV.36)}$$

within the steady state, the amplitude of the drift magnitude S is only determined (since one can assume that, due to the very low value of the conductivity of the silica layer compared to LN substrate, $R_{\text{sil}} \ll R_x, R_z$) by the relative ratio of the resistances associated with the LN substrate, and thus, according to the relation $R = (\rho L)/(S)$, where L and S are the thickness and the surface section of the considered layer, respectively, in a first approximation (assuming that the thickness and surface section are nearly the same in each layer), to the relative resistivity anisotropy ratio $(\rho_x)/(\rho_x + \rho_z)$ of the LN substrate. Within the short-time range, the drift magnitude S is only determined (since one can assume that, due to the very thin thickness of the layer, $C_{\text{sil}} \gg C_x, C_z$) by the relative ratio of the capacitances associated with the LN substrate, and thus, according to the relation $C = (\epsilon_0 \epsilon S)/(L)$, in a first approximation (assuming that the thickness and surface section are nearly the same in each layer), to the relative dielectric permittivity anisotropy ratio $(\epsilon_z)/(\epsilon_z + \epsilon_x)$ of the LN substrate.

ACKNOWLEDGMENT

The authors would like to thank H. Porte from *Photline Technologies* for providing them the LN MZI modulator, M. Mostefa and R. Ferriere from *FEMTO-ST* for supplying Ti in-diffused waveguides, and Prof. G. Montemezzani for useful discussion.

REFERENCES

[1] G. L. Li and P. K. L. Yu, "Optical intensity modulators for digital and analog applications," *J. Lightw. Technol.*, vol. 21, no. 9, pp. 2010–2030, Sep. 2003.

[2] H. Nagata and J. Ichikawa, "Progress and problems in reliability of TI:$LiNbO_3$ optical intensity modulators," *Opt. Eng.*, vol. 34, no. 11, pp. 3284–3293, 1995.

[3] S. K. Korotky and J. Veselka, "An *RC* network analysis of long term TI:$LiNbO_3$ bias stability," *J. Lightw. Technol.*, vol. 14, no. 12, pp. 2687–2697, Dec. 1996.

[4] G. E. Betts, C. H. Cox, and K. G. Ray, "20 GHz optical analog link using an external modulator," *IEEE Photon. Technol. Lett.*, vol. 2, no. 12, pp. 923–925, Dec. 1990.

[5] N. Miyazaki, K. Ooizumi, T. Hara, M. Yamada, H. Nagata, and T. Sakane, "TI:$LiNbO_3$ optical intensity modulator packaged with monitor photodiode," *IEEE Photon. Technol. Lett.*, vol. 13, no. 5, pp. 442–444, May 2001.

[6] Technical Note, ATT Microelectronics 1995, Lithium niobate modulators.

[7] D. Maack, "Reliability of lithium niobate Mach–Zehnder modulators for digital optical fiber telecommunications systems," in *Proc. SPIE Crit. Rev.: Reliabil. Opt. Fibers Opt. Fibers Syst.*, 1999, pp. 197–230.

[8] H. Nagata and H. Honda, "Initial bias dependency in dc drift of z-cut TI:$LiNbO_3$ optical intensity modulators," *Opt. Eng.*, vol. 39, no. 4, pp. 1103–1105, 2000.

[9] W. Minford, "The taming of TI:$LiNbO_3$," in *FIO III*, 1999.

[10] H. Nagata and K. Kiuchi, "Temperature dependence of dc drift of TI:$LiNbO_3$ optical modulators with sputter deposited SiO_2 buffer layer," *J. Appl. Phys.*, vol. 73, no. 9, pp. 4162–4164, 1993.

[11] H. Nagata, Y. Li, I. Croston, D. R. Maack, and A. Appleyard, "DC drift activation energy of TI:$LiNbO_3$ optical modulators based on thousands of hours of active accelerated aging tests," *IEEE Photon. Technol. Lett.*, vol. 14, no. 8, pp. 1076–1078, Aug. 2002.

[12] S. Yamada and M. Minakata, "DC drift phenomena in TI:$LiNbO_3$ optical waveguide devices," *Jpn. J. Appl. Phys.*, vol. 20, no. 4, pp. 733–737, 1981.

[13] R. A. Becker, "Circuit effect in TI:$LiNbO_3$ channel-waveguide modulators," *Opt. Lett.*, vol. 10, no. 8, pp. 417–419, 1985.

[14] H. Nagata, K. Kiuchi, S. Shimotsu, J. Ogiwara, and J. Minowa, "Estimation of direct current bias and drift of TI:$LiNbO_3$ optical modulators," *J. Appl. Phys.*, vol. 76, no. 3, pp. 1405–1408, 1994.

[15] H. Nagata, T. Kitanoubou, K. Shima, and M. Shiroishi, "Process control for a SiO_2 buffer layer of TI:$LiNbO_3$ modulators to obtain reduced DC drift performance," *Opt. Eng.*, vol. 36, no. 12, pp. 3478–3480, 1997.

[16] H. Nagata, H. Takahashi, H. Takai, and T. Kugo, "Impurity evaluation of SiO_2 films on TI:$LiNbO_3$ substrates," *Jpn. J. Appl. Phys.*, vol. 34, pp. 606–609, 1995.

[17] D. S. Kim, W. S. Yang, W. K. Kim, H. Y. Lee, H. Kim, and D. H. Yoon, "DC drift suppression of TI:$LiNbO_3$ waveguide chip by minimizing the contamination in oxide buffer layer," *J. Cryst. Growth*, vol. 288, pp. 188–191, 2006.

[18] H. Nagata, Y. Miyama, K. Higuma, Y. Hashimoto, F. Ya-mamoto, Y. Yamane, and M. Yatsuki, "Interface reactions in TI:$LiNbO_3$ based optoelectronic devices," in *Proc. Mat. Res. Soc. Symp.*, 2001, vol. 654, pp. AA321–AA325.

[19] H. Nagata, M. Shiroishi, T. Kitanoubou, and K. Ogura, "DC drift reduction in TI:$LiNbO_3$ optical modulators by decreasing the water content of vacuum evaporation deposited SiO_2 buffer layers," *Opt. Eng.*, vol. 37, no. 10, pp. 2855–2858, 1998.

[20] "," U.S. Patent 10 050 656.

[21] "," U.S. Patent 6 282 356.

[22] Y. Zhang, L. Guilbert, and P. Bourson, "Characterization of TI:$LiNbO_3$ waveguides by micro-Raman and luminescence spectroscopy," *Appl. Phys. B*, vol. 78, pp. 355–366, 2004.

[23] R. C. Twu, H. Y. Hong, and H. H. Lee, "An optical homodyne technique to measure photorefractive-induced phase drifts in lithium niobate phase modulators," *Opt. Exp.*, vol. 16, pp. 4366–4374, 2008.

[24] E. L. Wooten, K. M. Kissa, Y. Yan, E. J. Murphy, D. A. Lafaw, P. F. Hallemeier, D. Maack, D. V. Attanasio, D. J. Fritz, G. J. MacBrien, and D. E. Bossi, "A review of lithium niobate modulators for fiber-optic communications systems," *IEEE J. Sel. Topics Quantum Electron.*, vol. 6, no. 1, pp. 69–82, Jan./Feb. 2000.

[25] M. Powel and A. O'Donnell, "What integrated optics is really used for," *Opt. Photon. News*, vol. 8, pp. 23–28, 1997.

[26] "," U.S. Patent 6 198 855.

[27] H. Nagata, N. F. O'Beirn, W. R. Bosenberg, G. L. Reiff, and K. R. Voisine, "DC voltage-induced thermal shift of bias point in TI:$LiNbO_3$ optical modulators," *IEEE Photon. Technol. Lett.*, vol. 16, no. 11, pp. 2460–2462, Nov. 2004.

[28] M. Seino, T. Nakazawa, Y. Kubota, M. Doi, T. Yamane, and H. Hakogi, "A low DC drift TI:$LiNbO_3$ modulators assured over 15 years," in *Proc. Opt. Fiber Commun.*, 1992, pp. 325–328.

[29] P. Skeath, C. H. Bulmer, S. C. Hiser, and W. K. Burns, "Novel electrostatic mechanism in the thermal instability of z-cut TI:$LiNbO_3$ interferometers," *Appl. Phys. Lett.*, vol. 49, no. 19, pp. 1221–1223, 1986.

[30] "," U.S. Patent 6 044 184.

[31] R. V. Schmidt, P. S. Cross, and A. M. Glass, "Optically induced crosstalk in TI:$LiNbO_3$ waveguide switches," *J. Appl. Phys.*, vol. 51, no. 1, pp. 90–93, 1979.

[32] G. E. Betts, F. J. O'Donnel, and K. G. Ray, "Effect of annealing on photorefractive damage in titanium-indiffused $LiNbO_3$ modulators," *IEEE Photon. Technol. Lett.*, vol. 6, no. 1, pp. 211–213, 1994.

[33] R. A. Becker, "Thermal fixing of Ti-indifused $LiNbO_3$ channel waveguides for reduced photorefractive susceptibility," *Appl. Phys. Lett.*, vol. 45, pp. 121–123, 1984.

[34] H. Nagata, K. Kiuchu, and T. Sugamata, "Refractive index fluctuations in deformed TI:$LiNbO_3$ waveguides due to SiO_2 overlayer deposition," *Appl. Phys. Lett.*, vol. 63, pp. 1176–1178, 1993.
[35] U. Schlarb and K. Betzler, "Refractive indexes of lithium niobate as a function of temperature, wavelength, and composition: A generalized fit," *Phys. Rev. B.*, vol. 48, no. 21, pp. 15613–15620, 1993.
[36] M. Abarkan, M. Aillerie, J. P. Salvestrini, M. D. Fontana, and E. P. Kokanyan, "Electro-optic and dielectric properties of hafnium-doped congruent lithium niobate crystals," *Appl. Phys. B.*, vol. 92, pp. 603–608, 2008.
[37] A. M. Glass, D. von der Linde, and T. Negran*, Appl. Phys. Lett.*, vol. 25, p. 233, 1974.
[38] F. Nitanda, Y. Furukawa, S. Makio, M. Sato, and K. Ito, "Increased optical damage resistance and transparency in MgO-doped LITAO3 single crystals," *Jpn. J. Appl. Phys.*, vol. 34, pp. 1546–1549, 1995.
[39] M. Aillerie, M. D. Fontana, F. Abdi, C. Carabatos-Nedelec, N. Theofanous, and G. Alexakis*, J. Appl. Phys.*, vol. 65, no. 6, pp. 2406–2408, 1989.
[40] T. Bartholomaus, K. Buse, C. Deuper, and E. Kratzig*, Phys. Stat. Sol. (a)*, vol. 142, p. 55, 1994.
[41] J. de Toro, M. Serrano, A. G. Cabanes, and J. Cabrera, "Accurate interferometric measurement of electro-optic coefficients: Application to quasi-stoichiometric $LiNbO_3$," *Opt. Commun.*, vol. 154, p. 23, 1998.
[42] M. Jazbinsek and M. Zgonik, "Material tensor parameters of $LiNbO_3$ relevant for electro-and elasto-optics," *App. Phys. B.*, vol. 74, pp. 407–414, 2002.
[43] F. Giustino, P. Umari, and A. Pasquarello, "Dielectric effect of a thin SiO_2 interlayer at the interface between silicon and high-k oxides," *Microelectron. Eng.*, vol. 72, pp. 299–303, 2004.